Supplementary Material

Interfacial engineering between SnO₂/MAPbI₃ by maleate pheniramine halides toward carbon counter electrode-based perovskite solar cell with 16.21% efficiency

Duoling Cao[a,‖], Zuhong Li[a,‖], Wenbo Li[a], Ke Pei[a], Xu Zhang[*,a], Li Wan[*,a], Li Zhao[a], Alexey Cherevan[b], Dominik Eder[b], Shimin Wang[*,a]

[a]Key Laboratory for the Green Preparation and Application of Functional Materials, Ministry of Education, Hubei Key Laboratory of Polymer Materials, Hubei Collaborative Innovation Center for Advanced Organic Chemical Materials, Faculty of Materials Science and Engineering, Hubei University, Wuhan 430062, PR China.
[b]Institute of Materials Chemistry, Technische Universität Wien, Getreidemarkt 9/165, 1060 Vienna, Austria.

[*]Corresponding authors

E-mail address: wanli@hubu.edu.cn, wanli1983_3@aliyun.com (L. Wan)

E-mail address: xuzhang@hubu.edu.cn (X. Zhang)

E-mail address: shiminwang@126.com (S. Wang)

1. Experimental section

1.1. Materials

All chemical reagents were directly used without further purification. Lead iodide (PbI_2, 99.99%) and methylammonium iodide (MAI, 99.5%) were purchased from Xi'an Polymer Light Technology Co. SnO_2 colloid solution was obtained from Infinity Scientific Co., Ltd. Acetone (99.5%), ethyl alcohol (EA, 99.7%) and isopropyl alcohol (IPA, 99.7%) were gained from Sinopharm Group Chemical Reagent Co., Ltd. Chlorphenamine maleate (CHM, 99%), brompheniramine maleate (BHM, 98%), chlorobenzene (CB, 99.5%), dimethyl-sulfoxide (DMSO, 99.9%), and N,N-dimethyl-formamide (DMF, 99.9%) were bought from Aladdin Bio-Chem Technology Co., Ltd. Low-temperature conductive carbon paste was acquired from Shanghai Maituowei Technology Co., Ltd.

1.2. Device Fabrication

The fluorine-doped tin oxide (FTO) glass was sequentially washed with detergent, deionized water, acetone, EA, and IPA in an ultrasonic for each 20 min, and dried in a hot stream. Then, the FTO substrates were treat by UV-ozone for 20 min. The SnO_2 colloidal solution was spin-coated on the FTO substrate at 1,000 rpm for 6s and 4,000 rpm for 30 s, and the SnO_2 film was annealed at 150 °C for 30 min. Then, the SnO_2 films were treated with UVO for 15 min. Subsequently, different concentrations of CHM (6, 12, 18, and 24 mg mL^{-1}) and BHM (5, 10, 15, 20, and 25 mg mL^{-1}) solution were prepared by dissolving them in ethanol, respectively. For modified ETLs, the as-prepared modifier

solution was dynamically spin-coated on the SnO_2 films at 4,000 rpm for 30 s, and then annealed at 150 °C for 10 min. For the 1.8 M MAPbI$_3$ composition, MAI (0.2880g) and PbI$_2$ (0.8298g) were dissolved in the DMF/DMSO mixed solvents (9:1, V_{DMF}: V_{DMSO}). The as-prepared perovskite precursor solution was spin-coated on the pristine and modified SnO_2 films at 4,000 rpm for 30 s, and 100 µL of CB antisolvent was dripped on perovskite films at 14 s before ending the program. The wet perovskite films were followed by thermal annealing at 100 °C for 10 min. Finally, the carbon CE was prepared by screen printing, followed by drying at 100 °C for 15min.

1.3. Instruments and Characterization

X-ray diffraction (XRD) patterns were measured with a Bruker-AXS D8 Advance X-ray diffractometer using Cu K$_{\alpha1}$ radiation at 40 mA and 40 kV in the 2θ range of 5° to 60°. The structures and elemental states of the samples were analyzed by Fourier transform infrared spectroscopy (FTIR, Nicolet iS10) and X-ray photoelectron spectroscopy (XPS, ESCALAB 250Xi), respectively. Scanning electron microscope images were acquired using a field-emission scanning electron microscope (FESEM, 500 series: Sigma). The absorption spectrum of the perovskite film and the transmittance of electron transport layer were obtained by an UV-vis spectrophotometer. Photoluminescence (PL) and time-resolved photoluminescence (TRPL) spectroscopy measurements were obtained by a Fluo Time 300 (Pico Quant Ltd, 20.0 MHZ). Photocurrent density–voltage (J–V) curves were measured using a Keithley 2400 source meter

under simulated air-mass 1.5 global (AM 1.5G) illumination (100 mW·cm^{-2}) provided by a solar simulator (Oriel, model 91192-1000) with scan rate of 0.1 V s^{-1}. The incident photon-to-electron conversion efficiency (*IPCE*) of the PSCs was measured with a 300 W xenon lamp (Newport 66984). Water contact angles were obtained using a contact angle measuring instrument (POWEREACH, JC2000D1).

2. Figure section
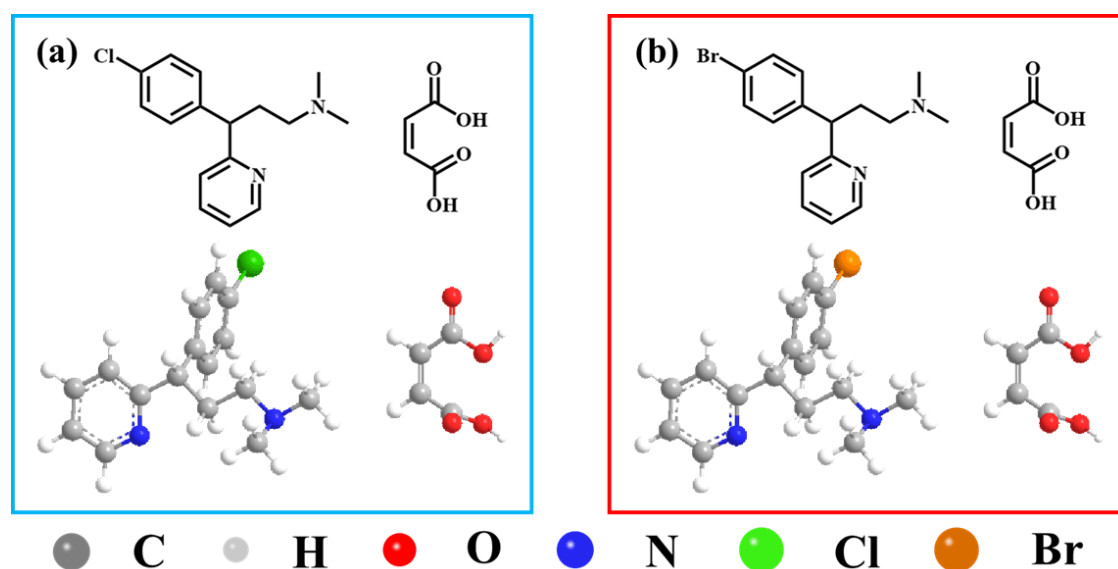
Fig. S1 The 2D molecular structure schematic and the optimizing of geometries of (a) CHM and (b) BHM.
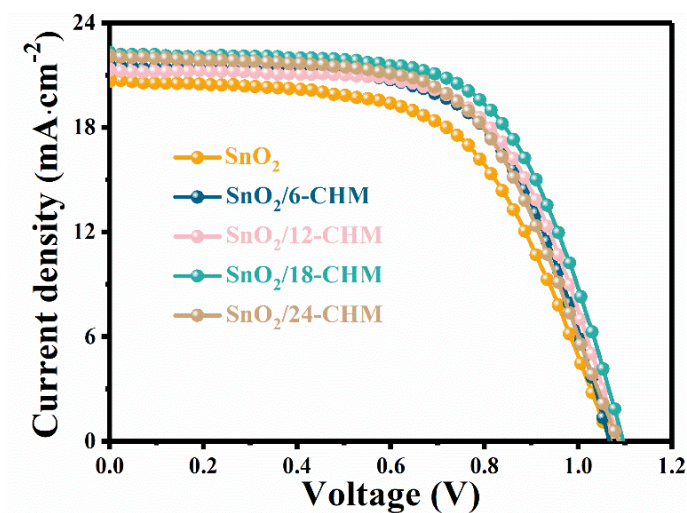
Fig. S2 *J-V* curves in reverse scan of the optimal PSCs based on SnO_2 with different concentration of CHM from 6 to 24 mg mL^{-1} compared with pristine SnO_2 ETLs. The scan rate is 0.1 V·s^{-1} under AM 1.5G illumination.
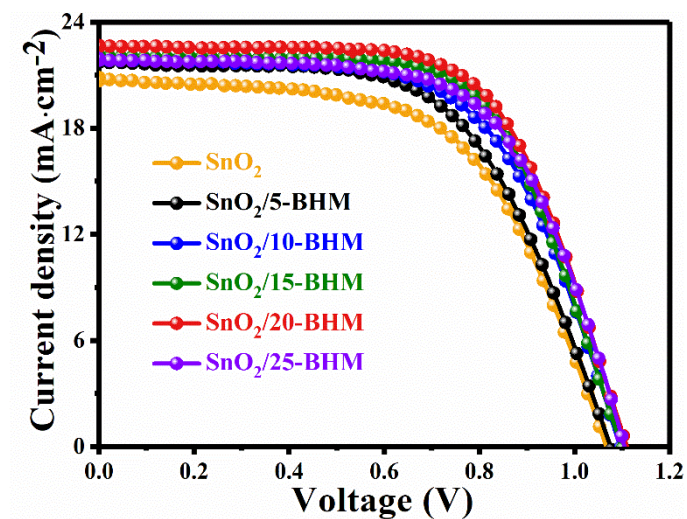
Fig. S3 *J-V* curves in reverse scan of the optimal PSCs based on SnO_2 with different concentration of BHM from 5 to 25 mg mL^{-1} compared with pristine SnO_2 ETLs. The scan rate is 0.1 V·s^{-1} under AM 1.5G illumination.

(a) **(b)**

(c) **(d)**

Fig. S4 (a) *PCE*, (b) V_{OC}, (c) J_{SC}, and (d) FF statistical diagrams of the devices modified by CHM and BHM compared with pristine SnO_2 ETLs. The statistical data were obtained from 40 individual cells.

(a)   (b)

(c)   (d)

Fig. S5 XPS spectra of (a) Full-scan and (b) N 1s of bare SnO_2, SnO_2/CHM, and SnO_2/BHM films. (c) Cl 2p XPS spectra of CHM and SnO_2/CHM films. (d) Br XPS spectra of BHM and SnO_2/BHM films.
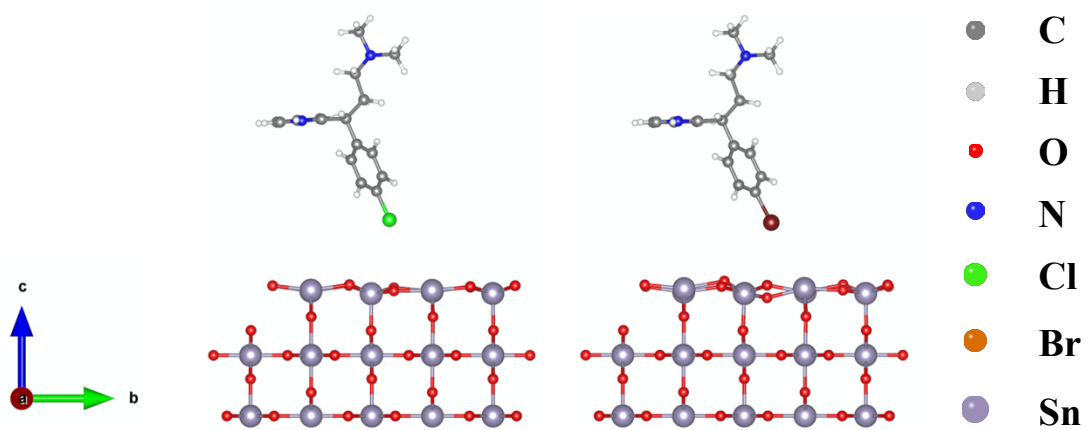
Fig. S6 Complexation energies of composites with SnO_2. The complexation energy of CHM-SnO_2 is -0.24eV, and that of BHM-SnO_2 is -0.42eV. The more negative value of complexation energy leads to the more stable complex.
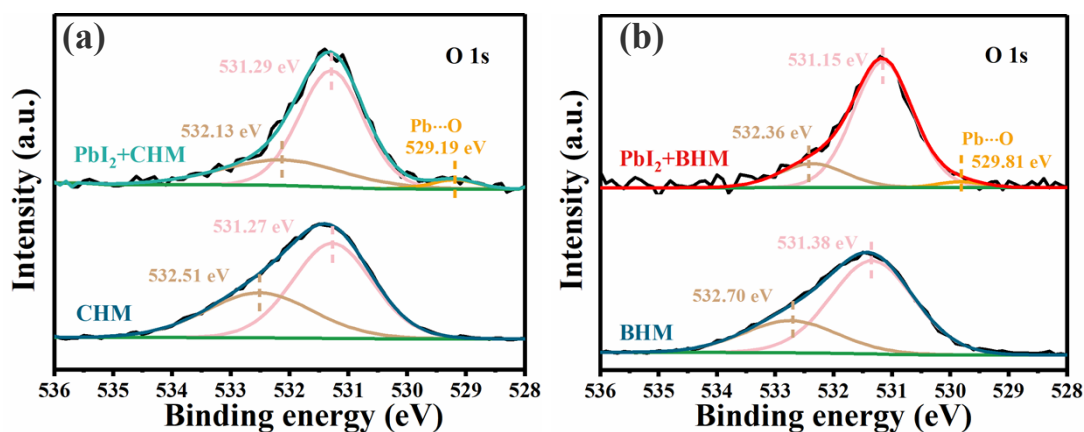
Fig. S7 (a) O 1s XPS spectra of CHM, PbI$_2$ with CHM. The two bonds signal of O-C=O (532.51 eV), C=O (531.27 eV) for O 1s spectra were found in pure CHM sample. For PbI$_2$ with CHM, the spectra of O 1s was deconvoluted into three peaks at 532.13, 532.29, and 529.19 eV, which were confirmed to O-C=O, C=O, and Pb-O, respectively. (b) O 1s XPS spectra of BHM, PbI$_2$ with BHM. For pure BHM sample, the spectra of O 1s was deconvoluted into two peaks at 532.70 and 531.38 eV, which were confirmed to O-C=O and C=O, respectively. For PbI$_2$ with BHM, the spectra of O 1s was deconvoluted into three peaks at 532.36, 532.15, and 529.81 eV, which were confirmed to O-C=O, C=O, and Pb-O, respectively.
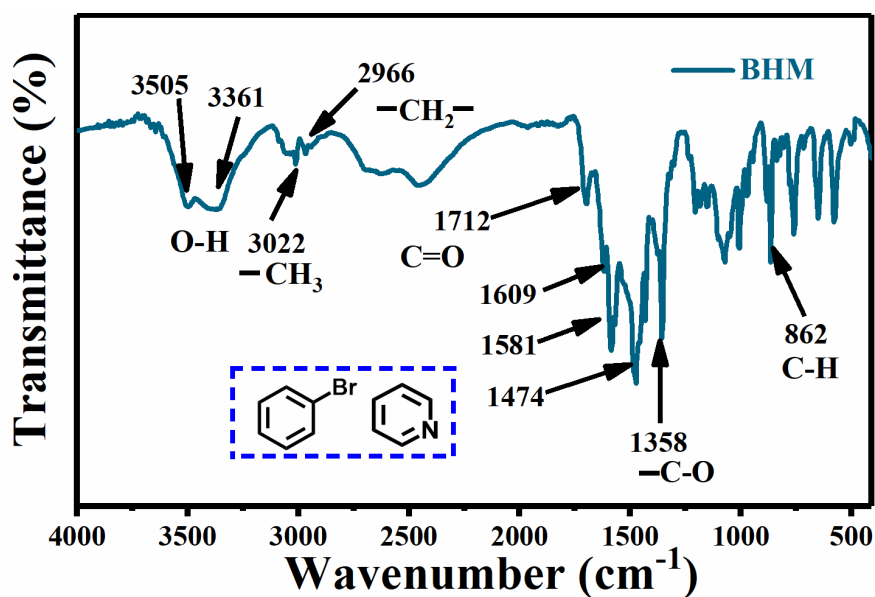
Fig. S8 FTIR spectrum of pure BHM powder. The O-H stretching vibration in maleic acid is around 3505 and 3361 cm⁻¹. The peaks around 3022 and 2966 cm⁻¹ belong to -C-H stretching vibration. The C=O stretching vibration peak is located at 1712 cm⁻¹. The characteristic absorptions of the benzene-ring and pyridine at 1600, 1550, and 1450 cm⁻¹. The peaks at 1550 and 1412 cm⁻¹ are attributed to -O-C=O stretching vibration. Additionally, the peak near 862 cm⁻¹ belongs to -C-H bending vibration.

(a)   **(b)**

Fig. S9 (a) FTIR spectra of film samples of SnO_2, CHM, and the SnO_2-CHM mixtures in the range of 1800 to 400 cm^{-1}. (b) FTIR spectra of film samples of PbI_2, CHM, and PbI_2-CHM mixtures in the range of 1800 to 400 cm^{-1}. The mixed solvent without pre-treatment has been subtracted for clarity of presentation.
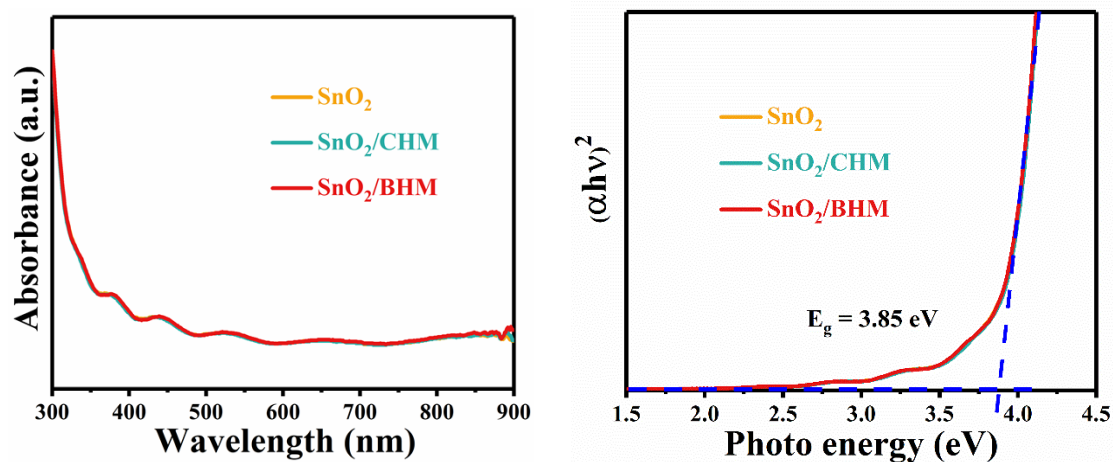
Fig. S10 Tauc plot spectra of SnO_2, SnO_2/CHM, and SnO_2/BHM are calculated form the UV-vis absorption spectra.
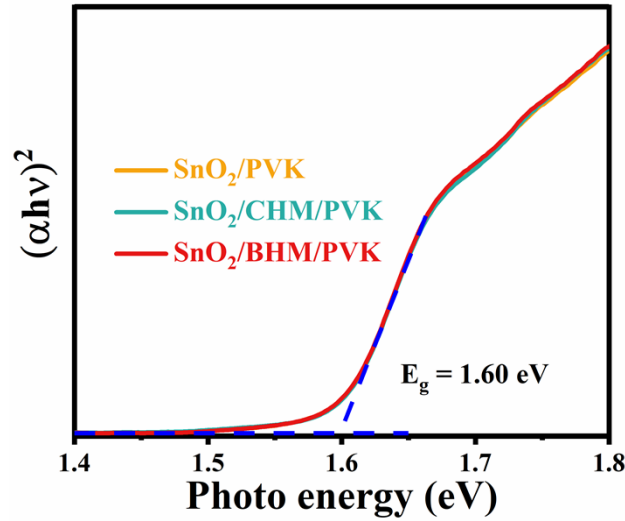
Fig. S11 The bandgap of perovskite films deposited on SnO_2, SnO_2/CHM, and SnO_2/BHM substrates form UV-vis absorption spectra. The optical bandgap is estimated by Tauc plot based on a direct bandgap transition relation $(\alpha h \nu)^2 = B(h\nu - E_g)$, where α is the absorption coefficient, $h\nu$ is the photon energy (21.22 eV), and E_g is the bandgap energy.
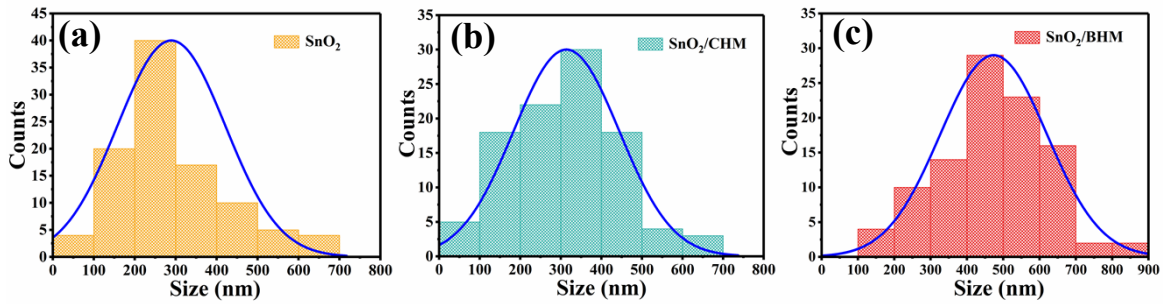
Fig. S12 The distribution diagram with an average grain size of the perovskite (a) without modified, (b) with CHM treatment, and (c) with BHM treatment.
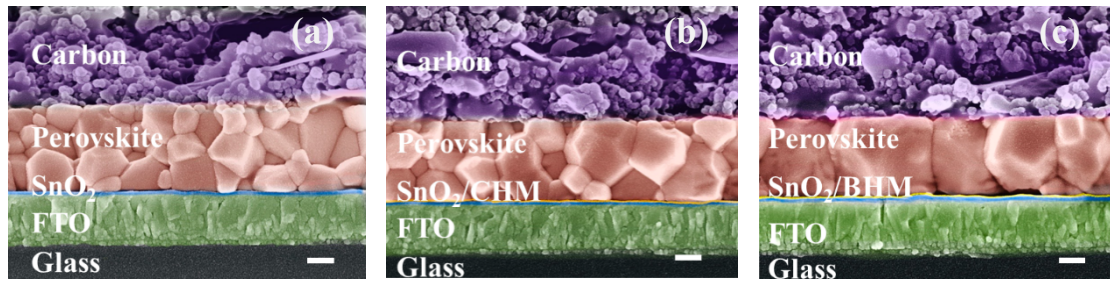
Fig. S13 The cross-sectional SEM images for rigid devices (a) without modified, (b) with CHM treatment, and (c) with BHM treatment; the scale bar is 200 nm.
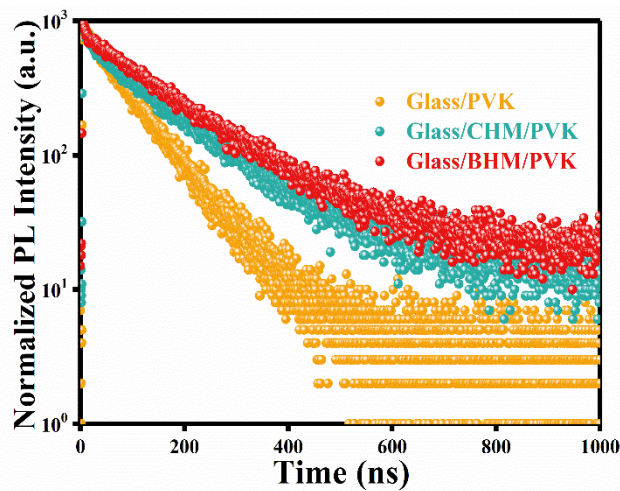
Fig. S14 TRPL spectra of perovskite films on the Glass, Glass/CHM and Glass/BHM substrates.
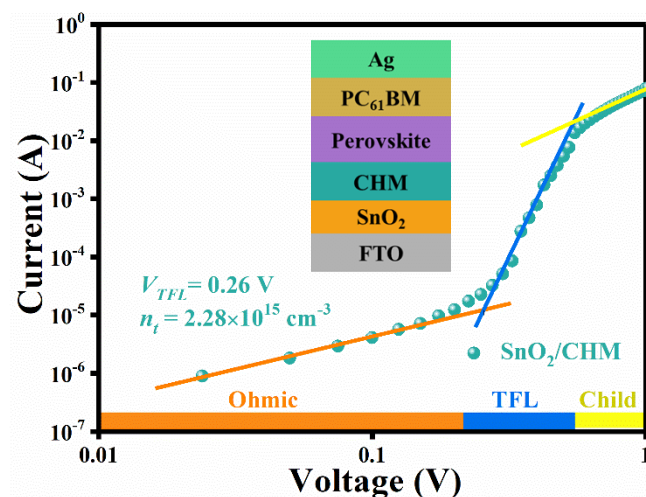
Fig. S15 Dark *I-V* curves of the electron-only devices with a configuration of FTO/SnO$_2$/CHM/MAPbI$_3$/PCBM/Au.
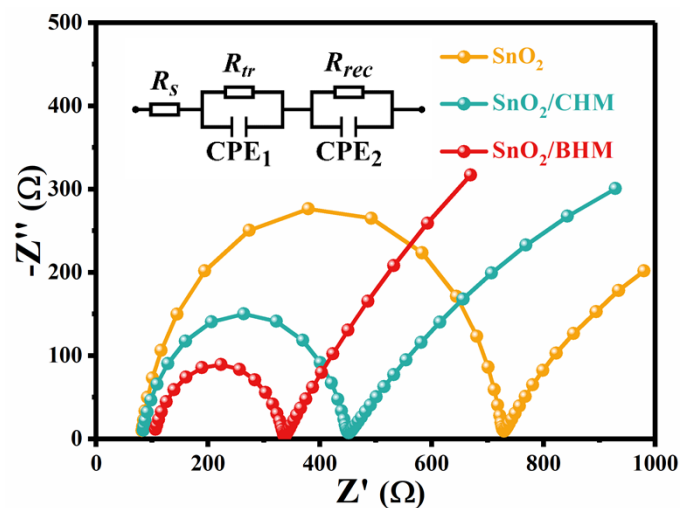
Fig. S16 Nyquist plots of PSCs based on SnO$_2$, SnO$_2$/CHM, and SnO$_2$/BHM. The inset shows the equivalent circuit diagram.

3. Table section

Table S1 Performances of PSCs based on SnO_2 and CHM passivated counterparts in Fig. S2. *J-V* curves were measured with a scan rate of 0.1 V s^{-1} under AM 1.5G illumination

Concentration (mg·mL^{-1})	V_{OC} (V)	J_{SC} (mA·cm^{-2})	FF	PCE (%)
0	1.066	20.82	0.59	13.04
6	1.066	21.55	0.63	14.44
12	1.078	21.33	0.64	14.70
18	1.089	22.3	0.64	15.47
24	1.078	22.13	0.61	14.52

Table S2 Photovoltaic parameters of PSCs based on unmodified and CHM modified SnO_2 with different concentration from 5 to 25 mg mL^{-1} in Fig. S3. *J-V* curves were measured with a scan rate of 0.1 V s^{-1} under AM 1.5G illumination

Concentration (mg·mL^{-1})	V_{OC} (V)	J_{SC} (mA·cm^{-2})	FF	PCE (%)
0	1.066	20.82	0.59	13.04
5	1.066	21.83	0.60	13.90
10	1.088	21.93	0.62	14.74
15	1.089	22.07	0.65	15.71
20	1.103	22.63	0.65	16.21
25	1.099	21.88	0.64	15.33

Table S3 Performance summary of the champion devices based on SnO_2 and SnO_2 passivated with CHM and BHM in Fig. 1c (Data in brackets are the average values of each parameter for 40 devices). *J-V* curves were measured with a scan rate of 0.1 V·s^{-1} under AM 1.5G illumination

PSC samples	V_{OC} (V)	J_{SC} (mA·cm^{-2})	FF	PCE (%)
SnO_2	1.068±0.01 （1.078）	21.05±0.66 （22.11）	0.58±0.03 （0.61）	13.12±0.79 （13.97）
SnO_2/CHM	1.087±0.01 （1.09）	22.00±0.71 （22.76）	0.61±0.03 （0.64）	15.14±0.58 （15.87）
SnO_2/BHM	1.104±0.01 （1.103）	22.65±054 （23.23）	0.63±0.02 （0.65）	15.60±0.55 （16.20）

Table S4 Summary of state-of-the-art HTM-free carbon CE-based $MAPbI_3$ perovskite solar cells

Device configuration	V_{OC} (V)	J_{SC} (mA·cm^{-2})	FF	PCE (%)	Reference
FTO/SnO$_2$/MAPbI$_3$(PFTeDA)/Carbon	1.10	23.85	0.718	18.9	10 in main text
FTO/SnO$_2$/BHM/MAPbI$_3$/Carbon	1.103	22.63	0.65	16.21	This work
FTO/SnO$_2$/CHM/MAPbI$_3$/Carbon	1.089	22.3	0.64	15.47	This work
ITO/SnO$_2$/MAPbI$_3$/Carbon	1.021	23.29	0.657	15.62	[1]
FTO/SnO$_2$/AMIMOAc/MAPbI$_3$ (AMIMOAc)/Carbon	1.084	22.18	0.631	15.16	[2]
FTO/SnO$_2$/MAPbI$_3$(*p*-MePMAI) /Carbon	1.078	21.37	0.632	14.54	[3]
FTO/TiO$_2$/MAPbI$_3$/Carbon-PGMEA	1.05	20.25	0.63	13.5	[4]

Table S5 TRPL fitting parameters of perovskite films deposited on SnO_2, SnO_2/CHM and SnO_2/BHM substrates in Fig. 5b

Samples	A_1 (%)	τ_1 (ns)	A_2 (%)	τ_2 (ns)	τ_{ave} (ns)
FTO/SnO₂/PVK	1.042	247.3	-0.62	225	273.62
FTO/SnO₂/CHM/PVK	0.62	186.9	0.127	106	178.48
FTO/SnO₂/BHM/PVK	0.67	93.28	0.13	21.3	90.23

Table S6. TRPL fitting parameters of perovskite films deposited on the Glass, Glass/CHM and Glass/BHM substrates form Fig. S14

Samples	A_1 (%)	τ_1 (ns)	A_2 (%)	τ_2 (ns)	τ_{ave} (ns)
Glass/PVK	0.771	86.9	0.117	19.1	84.71
Glass/CHM/PVK	0.6274	147.13	0.1543	20.4	142.95
Glass/BHM/PVK	0.7231	157	0.023	30	156.23

Table S7 The fitting results of EIS spectra of PSCs based on SnO_2 and SnO_2 passivated with CHM and BHM in Fig. S16

PSC samples	R_s (Ω)	R_{tr} (Ω)	R_{rec} (Ω)
SnO₂	80.48	645.3	890
SnO₂/CHM	81.8	365.7	1795
SnO₂/BHM	102.6	233.3	2500

References

1. S. Iqbal, H. Xie, X. Yin, Y. Guo, C. Zhang, D. Liu, B. Wang, B. Gao and W. Que, Methylamine-based method to deposit $MAPbI_3$ nanoscale-thick films for efficient perovskite solar cells with carbon electrodes, *ACS Appl. Nano Mater.*, 2022, **5**, 4112-4118.

2. Y. Huang, H. Zhong, W. Li, D. Cao, Y. Xu, L. Wan, X. Zhang, X. Zhang, Y. Li, X. Ren, Z. Guo, X. Wang, D. Eder and S. Wang, Bifunctional ionic liquid for enhancing efficiency and stability of carbon counter electrode-based $MAPbI_3$ perovskites solar cells, *Sol. Energy.*, 2022, **231**, 1048-1060.

3. Y. Xu, Y. Huang, H. Zhong, W. Li, D. Cao, C. Zhang, H. Bao, Z. Guo, L. Wan, X. Zhang, X. Zhang, Y. Li, X. Wang, D. Eder and S. Wang, Enhanced performance and stability of carbon counter electrode-based $MAPbI_3$ perovskite solar cells with p-methylphenylamine iodate additives, *ACS Appl. Energy Mater.*, 2021, **4**, 11314-11324.

4. Q.-Q. Chu, B. Ding, Q. Qiu, Y. Liu, C.-X. Li, C.-J. Li, G.-J. Yang and B. Fang, Cost effective perovskite solar cells with a high efficiency and open-circuit voltage based on a perovskite-friendly carbon electrode, *J. Mater. Chem. A*, 2018, **6**, 8271-8279.